

Hydrodynamic Simulations of Merging Galaxy Clusters: Non-Equilibrium Ionization State and Two-Temperature Structure

Takuya AKAHORI¹ and Kohji YOSHIKAWA²

¹*Research Institute of Basic Science, Chungnam National University, Daejeon 305-764, Korea*

akataku@canopus.cnu.ac.kr

²*Center for Computational Sciences, University of Tsukuba, 1-1-1, Tennodai, Tsukuba, Ibaraki 305-8577*

kohji@ccs.tsukuba.ac.jp

(Received 2009 September 21; accepted)

Abstract

We investigate a non-equilibrium ionization state and an electron-ion two-temperature structure of the intracluster medium in merging galaxy clusters using a series of N-body and hydrodynamic simulations. Mergers with various set of mass ratios and impact parameters are systematically investigated, and it is found that, in most cases, the intracluster medium significantly departs from the ionization equilibrium state at the shock layers with a Mach number of ~ 1.5 – 2.0 in the outskirts of the clusters, and the shock layers with a Mach number of ~ 2 – 4 in front of the dense cores. Accordingly, the intensity ratio between Fe XXV and Fe XXVI $K\alpha$ line emissions is significantly altered from that in the ionization equilibrium state. If the effect of the two-temperature structure of the plasma is incorporated, the electron temperature is ~ 10 – 20 % and ~ 25 – 50 % lower than the mean temperature of the plasma at the shock layers in the outskirts and in front of the dense cores, respectively, and the deviation from the ionization equilibrium state becomes larger. We also address the dependence of the intensity ratio on the viewing angle with respect to the merging plane.

Key words: X-rays: galaxies: intergalactic medium — X-rays: galaxies: clusters

1. Introduction

Galaxy clusters host an X-ray emitting hot gas with temperature of $\sim 10^{7-8}$ K, or the intracluster medium (ICM), as well as dark matter and galaxies. It is theoretically believed that ICM has been heated up through various magnitude of shock waves caused by successive mergers of galaxies, galaxy groups and galaxy clusters during the hierarchical structure formation (e.g., Ryu et al. 2003). These shocks are regarded as sources of turbulent motion of ICM and sites of particle acceleration. Furthermore, they amplify the intracluster magnetic fields and can be sources of non-thermal emission. In this sense, merging galaxy clusters are of great importance as fruitful sites of interesting phenomena of astrophysical plasma (see Sarazin 2002 for a review).

From observational point of view, merging galaxy clusters provide lots of information about outskirts of galaxy clusters, because compression and shock heating of ICM during merging events increase the X-ray luminosity of ICM at the outer parts of galaxy clusters. For example, Fujita et al. (2008) reported the detection of Fe K emission lines in the linked region of Abell 399 and Abell 401, more than ~ 1 Mpc apart from the centers of both galaxy clusters, and estimated the metallicity relatively higher than conventionally expected, based on the Suzaku XIS observation. Their detection is in virtue of the fact that ICM in the linked region is significantly compressed, as well as the high sensitivity of the XIS detector. Therefore, merging galaxy clusters can be good sites for elucidating

physical properties of ICM, such as the temperature and metallicity, especially in the peripheral regions of galaxy clusters.

Measurements of physical properties of ICM, such as temperature and metallicity, in X-ray observations, however, usually assume that ICM is in the ionization equilibrium state, and that electrons and ions share the same thermal temperature. It is widely believed that these assumptions are reasonable inside galaxy clusters, because the timescale for collisional ionization equilibrium,

$$t_{\text{CIE}} \sim 3 \times 10^8 \text{ yr} \left(\frac{n_e}{10^{-3} \text{ cm}^{-3}} \right)^{-1}, \quad (1)$$

(e.g., Masai 1984) and the timescale for thermal equilibration between electrons and ions through Coulomb scattering,

$$t_{\text{ei}} \sim 2 \times 10^8 \text{ yr} \left(\frac{n_e}{10^{-3} \text{ cm}^{-3}} \right)^{-1} \left(\frac{T_e}{10^8 \text{ K}} \right)^{3/2}, \quad (2)$$

(Spitzer 1962) are usually shorter than the typical dynamical timescale around the central regions of galaxy clusters, where n_e and T_e are the number density and temperature of electrons, respectively. But these timescales are not short enough compared with the merger timescale, and even longer in the outskirts of galaxy clusters where $n_e \sim 10^{-4} \text{ cm}^{-3}$. Consequently, the assumptions of the ionization equilibrium and the thermal equipartition between electrons and ions are no longer justified. Therefore, in measuring the temperature and/or metallicity of ICM around shock layers and outskirts of merging galaxy clusters,

ters, the deviations from the ionization equilibrium and the thermal equipartition have to be taken into consideration.

Previously, many works were devoted to numerical simulations of merging galaxy clusters under idealized but well-controlled initial conditions (Roettiger, Loken, Burns 1997; Ricker, Sarazin 2001; Ritchie, Thomas 2002; Takizawa 2005; Takizawa 2006). But most of them ignored the effects of the non-equilibrium ionization state and the deviation from thermal equipartition between electrons and ions, or the two-temperature structure of ICM. Takizawa (1999) and Takizawa (2000) took into account the latter effect in numerical simulations of merging galaxy clusters for the first time, while Yoshida et al. (2005) and Rudd, Nagai (2009) investigated it in Warm–Hot Intergalactic Medium (WHIM) and in outskirts of galaxy clusters, respectively, in cosmological simulations. The former effect in WHIM is addressed in cosmological simulations for the first time by Yoshikawa, Sasaki (2006) and Cen, Fang (2006). Recently, Akahori, Yoshikawa (2008)(AY08) carried out an N-body/SPH simulation of Abell 399 and Abell 401 system incorporating these two effects simultaneously and self-consistently, and showed that the non-equilibrium ionization state and the two-temperature structure of ICM take place along shock layers at the merging interface.

While AY08 addressed only a particular situation of Abell 399 and Abell 401, in this paper, we systematically investigate the non-equilibrium ionization state and the two-temperature structure of ICM for various situations of merging galaxy clusters, e.g., mass ratios, impact parameters, and merging stages, so as to be confronted with future X-ray observations of actual merging galaxy clusters. In addition to that, we also address the viewing angle dependence of observational signatures of the deviation from the ionization equilibrium and the thermal equipartition.

The rest of this paper is organized as follows. In section 2, we describe the numerical methods and the initial conditions of the simulation. The results of the simulations are presented in section 3. In section 4, we summarize our conclusions and discuss the future prospects for the detection of non-equilibrium ionization states and the two-temperature structure of ICM. In the case that the cosmological scaling is required, we assume the density parameter $\Omega_M = 0.24$, the baryon density parameter $\Omega_b = 0.04$, and the Hubble constant $H_0 = 70 \text{ km s}^{-1} \text{ Mpc}^{-1}$, unless otherwise specified.

2. Simulation

2.1. Numerical Method

We carry out a set of N-body and SPH simulations of merging galaxy clusters for various initial conditions. In all simulations, radiative cooling is ignored, since, in this work, we focus on relatively outer regions rather than the very central regions of galaxy clusters, and the actual cooling timescale in the central regions of the simulated ICM is $\sim 5 \text{ Gyr}$, sufficiently longer than

the merging timescale. Simulations are performed using the code developed in the previous papers (Akahori, Masai 2005, Akahori, Masai 2006, and AY08), which adopts the entropy conservative formulation of SPH by Springel, Hernquist (2002), and the standard Monaghan-Gingold artificial viscosity (Monaghan, Gingold 1983) with Balsara limiter (Balsara 1995). In addition to the standard SPH prescription, the time evolution of the two-temperature structure and the non-equilibrium ionization state of the ICM are incorporated.

As for the time evolution of the two-temperature structure, only the Coulomb scattering is considered as a physical process responsible for the thermal relaxation between electrons and ions. In this picture, timescales on which each of electrons and ions achieves the thermal relaxation are much shorter than that between electrons and ions. Therefore, electrons and ions can have different temperatures, T_e and T_i , respectively, just after experiencing shock heating, because nearly all of the kinetic energy of ICM is carried by ions at a shock front, and is preferentially converted to the thermal energy of ions in the post-shock regions. Afterward, thermal relaxation between electrons and ions proceeds through Coulomb scattering on a timescale described by

$$t_{ei} = \frac{3m_e m_i}{8(2\pi)^{1/2} n_i Z_i^2 e^4 \ln \Lambda} \left(\frac{k_B T_e}{m_e} + \frac{k_B T_i}{m_i} \right)^{3/2} \quad (3)$$

$$\simeq 2 \times 10^8 \text{ yr} \frac{(T_e/10^8 \text{ K})^{3/2}}{(n_i/10^{-3} \text{ cm}^{-3})} \cdot \left(\frac{40}{\ln \Lambda} \right),$$

where m_e and m_i are the electron and ion mass, respectively, n_i the number density of ions, k_B the Boltzmann constant, and $\ln \Lambda$ the Coulomb logarithm (Spitzer 1962).

Assuming that electrons and ions share the same fluid velocity, and that shock heating are exclusively contributed to the heating of ions, the energy equations for electrons and ions are given as

$$\rho \frac{du_e}{dt} = -P_e \nabla \cdot v + Q_{\text{ex}}, \quad (4)$$

$$\rho \frac{du_i}{dt} = -P_i \nabla \cdot v + Q_{\text{sh}} - Q_{\text{ex}}, \quad (5)$$

respectively, where ρ is the gas mass density, u the specific thermal energy, P the thermal pressure (quantities with subscript “e” and “i” denote those of electrons and ions, respectively), Q_{sh} the shock heating rate per unit volume, and Q_{ex} the energy exchange rate per unit volume through Coulomb scattering:

$$Q_{\text{ex}} = \frac{n_e k_B}{\gamma - 1} \frac{T_i - T_e}{t_{ei}}, \quad (6)$$

where $\gamma = 5/3$ is the adiabatic index. Using equations (4) and (5), and assuming the constant mean molecular weight, $\mu = 0.6$, for almost fully ionized ICM, we obtain an ordinary energy equation for mixed fluid with a mean temperature $\bar{T} = (n_e T_e + n_i T_i)/(n_e + n_i)$, and another equation for the time evolution of electron temperature, which can be written as

$$\frac{d\tilde{T}_e}{dt} = \frac{\tilde{T}_i - \tilde{T}_e}{t_{ei}} - \frac{\tilde{T}_e}{u} Q_{sh}, \quad (7)$$

where $\tilde{T}_e \equiv T_e/\bar{T}$ and $\tilde{T}_i \equiv T_i/\bar{T}$ are the dimensionless temperatures of electrons and ions normalized by the mean temperature, respectively, and $u = u_e + u_i$. This equation is numerically solved in the same manner described in Takizawa (1999) as follows. We first regard the second term on the right hand side as being negligibly small, and integrate the first term implicitly using the method described in Fox, Loeb (1997). Then we integrate the second term explicitly, and finally add this contribution to the time evolution of \tilde{T}_e . In each integration, the time step regulated by the courant condition of SPH ensures sufficiently smaller Q_{sh}/u than unity and thus enable us to solve the evolution of \tilde{T}_e with reasonable accuracy.

Actually, a possibility is argued that plasma waves are able to attain the thermal relaxation between electrons and ions more quickly than the Coulomb collision. In reality, it is observationally suggested that the electron and ion temperatures are almost the same around the shock front with a Mach number of $\simeq 10 - 20$ in supernova remnants, indicating that physical processes other than Coulomb collision contribute to the quick thermal relaxation between electrons and ions (Ghavamian et al. 2007). There exists, however, a room for a very slow shock with a Mach number of $M \lesssim 5$ to have significant difference in the temperatures between electrons and ions. Thus, in order to bracket the plausible range of theoretical uncertainties, we present the results both for the two-temperature runs described above and the single-temperature runs, in which thermal energies of ions and electrons are assumed to be instantaneously equilibrated, and ions and electrons share the single temperature.

The time evolution of ionization fractions of ions is computed by solving the rate equation,

$$\begin{aligned} \frac{df_j}{dt} = & \sum_{k=1}^{j-1} S_{j-k,k} f_k - \sum_{i=j+1}^{Z+1} S_{i-j,j} f_j \\ & - \alpha_j f_j + \alpha_{j+1} f_{j+1}, \end{aligned} \quad (8)$$

for each SPH particle, where j is the index of a particular ionization stage considered, Z the atomic number, f_j the ionization fraction of an ion j , $S_{i,j}$ the ionization rate of an ion j with the ejection of i electrons, and α_j is the recombination rate of an ion j . The ionization processes include collisional, Auger, charge-transfer, and photo-ionizations, and recombination processes are composed of radiative and dielectronic recombinations. The ionization and recombination rates are calculated by utilizing the SPEX ver 1.10 software package¹.

Equation (8) is integrated implicitly in the same manner described in Yoshikawa, Sasaki (2006), in which ionization fractions of all ionic species are sequentially updated in the order of increasing ionization states rather than being updated simultaneously, and the source terms contributed by the ionization from and recombination to the lower

Table 1. Simulation runs and their merging parameters

run ID	$M_1 [M_\odot]$	$M_2 [M_\odot]$	$v_i [\text{km s}^{-1}]$	$b [\text{Mpc}]$
1:1 head on	10^{15}	10^{15}	1145	0.0
1:1 offset	10^{15}	10^{15}	1153	0.81
4:1 head on	10^{15}	2.5×10^{14}	1046	0.0
4:1 offset	10^{15}	2.5×10^{14}	1055	0.81

states are evaluated at the advanced time step. In the two-temperature runs, the reaction rates are computed using the electron temperature, T_e , calculated from equation (7) so as to incorporate the effect of the two-temperature structure. As for the single-temperature runs, the reaction rates are computed using the mean temperature, \bar{T} .

We solve the time evolution of the ionization fractions of H, He, C, N, O, Ne, Mg, Si, S, and Fe; total 112 ionization states for each SPH particle. All the ionization states are considered in calculations of the X-ray spectrum and the surface brightness in this paper. But in the following, we mainly focus on the ionization fraction and the line intensities of Fe, because the line emissions of Fe are the most prominent in the typical temperature range of ICM $\sim 10^7 - 8$ K.

2.2. Initial Condition

The initial conditions are setup as follows. We adopt the NFW density profile (Navarro, Frenk, White 1997) for a dark matter halo, and the β -model density profile (Cavaliere, Fusco-Femiano 1976) with $\beta = 0.6$ for a ICM component. The scale radius of the NFW profile is set to $r_s = r_{200}/4.07$, and the core radius of the β -model is $r_c = r_s/2$, where r_{200} is the virial radius defined as the radius within which the mean cluster mass density is 200 times the present cosmic critical density. The radial profiles of velocity dispersion of dark matter and temperature of ICM are computed using Jeans equation and the assumption of hydrostatic equilibrium, respectively. The gas and dark matter particles are distributed out to $1.4 r_{200}$, which enables us to follow the dynamical evolution of ICM at outskirts of galaxy clusters.

In this paper, mass ratios of two galaxy clusters are set to 1:1 and 4:1. For runs with 1:1 mass ratio, the virial mass and radius are set to $M_{200} = 1.0 \times 10^{15} M_\odot$ and $r_{200} = 1.63$ Mpc, respectively. For runs with 4:1 mass ratio, a main (or more massive) cluster is the same as the one in the runs with 1:1 mass ratio, and the virial mass and radius of a sub- (or less massive) cluster are set to $M_{200} = 2.5 \times 10^{14} M_\odot$ and $r_{200} = 1.03$ Mpc, respectively. Density profiles of dark matter and ICM and temperature profiles for the two masses of galaxy clusters are depicted in figure 1. For each mass ratio, we carry out the runs with different impact parameters b ; “head-on” runs with $b = 0$ and “off-set” runs with $b = 0.81$ Mpc. As for the metallicity, a spatially uniform metallicity of 0.2 times the solar abundance is assumed. In addition to that, we also as-

¹ <http://www.sron.nl/divisions/hea/spex/>

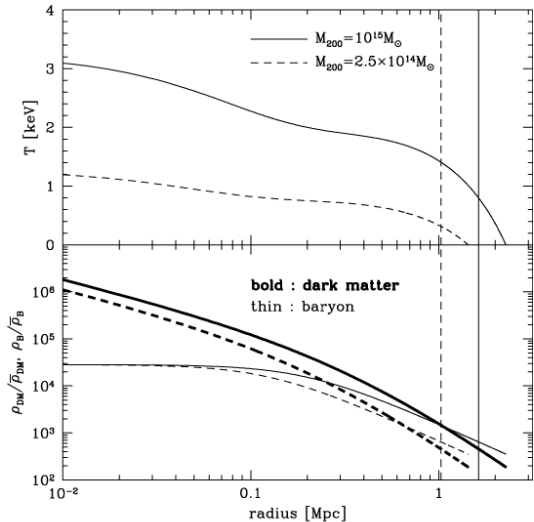


Fig. 1. Radial density profiles of ICM (baryon) and dark matter normalized by the cosmic mean density of each component (lower panel), and ICM temperature (upper panel) at initial conditions. Solid lines indicate the profiles of galaxy clusters in the runs with 1:1 mass ratio and the main cluster in the runs with 4:1 mass ratio ($M_{200} = 10^{15} M_{\odot}$), while dashed lines show the profiles of the sub-cluster in the runs with 4:1 mass ratio ($M_{200} = 2.5 \times 10^{14} M_{\odot}$). The vertical lines indicate the locations of their virial radii. The central ICM density corresponds to $n_e = 5.42 \times 10^{-3} \text{ cm}^{-3}$.

sume that electrons and ions share the same temperature, and that they are in the ionization equilibrium state at the start of the simulations.

The initial separation of two galaxy clusters, d , is set to 1.4 times of the sum of their virial radii so that they contact each other at their outer edge. The initial relative velocity of the two clusters, v_i , is calculated using the prescription described in Sarazin (2002), and is given by

$$v_i^2 = 2G(M_1 + M_2) \left(\frac{1}{d} - \frac{1}{d_0} \right) \left[1 - \left(\frac{b}{d_0} \right)^2 \right]^{-1}, \quad (9)$$

where G is the gravitational constant, and M_1 and M_2 are the virial masses of the two clusters. d_0 denotes the maximum separation where their relative *radial* velocity is zero, and is calculated with the aid of the Kepler's third law as follow

$$d_0 = [2G(M_1 + M_2)]^{1/3} \left(\frac{t_0}{\pi} \right)^{2/3}, \quad (10)$$

where t_0 is the comic time when the merging event takes place, and is set to $t_0 = 13.7$ Gyr in this paper. All the runs presented in this paper and their merging parameters are listed in table 1.

In all simulations, the mass of each dark matter and SPH particle is set to $1.10 \times 10^9 M_{\odot}$ and $2.19 \times 10^8 M_{\odot}$, respectively. The single cluster in the runs with 1:1 mass ratio, and the main cluster in the runs with 4:1 mass ratio are composed of one million dark matter particles and the same number of SPH particles, while the sub-clusters in

the runs with 4:1 mass ratio are represented by a quarter million particles for each component.

3. Result

3.1. Single-Temperature Runs

First, we show the results for the single-temperature runs, in which thermal relaxation between electrons and ions is supposed to be achieved very quickly, and electrons and ions share a single temperature.

Figure 2 shows the time evolution of the ICM density (color), the dark matter density (black contour), and the Mach number distribution of ICM (white contour), on a collision plane of the two merging galaxy clusters, where the Mach number is estimated with the shock-capture scheme described in Pfrommer et al. (2006). Panels from the top to the bottom show the snapshots at a time of $t = -0.8$ Gyr, 0.4 Gyr, and 1.0 Gyr, where $t = 0$ Gyr corresponds to the time of the closest approach of the centers of the dark matter halos.

In the early stage of the merging ($t = -0.8$ Gyr), the outskirts of the two galaxy clusters interact with each other, and then form the linked regions where ICM is compressed due to the collision. At the edges of the linked regions, there exist shock layers with a Mach number of 1.5–2.0 (white contour in the top panels of figure 2). These shocks are immediately generated at contact interface of the two clusters when the clusters start to collide, then propagate to outside of each cluster.

The emergence of these shocks at the outskirts of galaxy clusters is also pointed out by AY08, but not clearly seen in the previous SPH simulations (Takizawa 1999; Takizawa 2000). This is because, in these previous studies, density profiles of ICM are truncated in the outside of clusters ($r > 5r_c$), and also because these studies adopt isothermal temperature profiles of ICM at the start of the simulations. On the contrary, in the present study, the distributions of ICM are extended out to $r = 8.15r_c$, and the ICM temperature decreases toward outside as suggested by recent X-ray observations (e.g., Vikhlinin et al. 2005). Therefore, the sound speed at the outskirts of galaxy clusters, which is typically $\sim 500 \text{ km s}^{-1}$ for a gas temperature of $\sim 10^7 \text{ K}$, is lower than the relative velocity ($\sim 1000 \text{ km s}^{-1}$) of the two clusters, resulting in the formation of the shock waves.

At the middle stage of the merging ($t = 0.4$ Gyr), another shock waves with a Mach number of 1.5 – 2.0 in front of the ICM density peaks emerge, because the dense cores of ICM are accelerated by the preceding dark matter halos, and they have Mach numbers of $\sim 3 - 4$ and $2 - 2.5$ at the late stage of the merging ($t = 1.0$ Gyr) in the case of 1:1 and 4:1 mass ratios, respectively. Since the shock waves formed ahead of the ICM density peaks are faster than the ones formed in the outskirts at the early stage, the former overtake and merge with the latter, as can be seen in the bottom panels of figure 2.

As shown in the top panels of figure 3, most of ICM except the regions behind the shocks is in the temperature range of $2 \lesssim T \lesssim 7 \text{ keV}$, and in this temperature range,

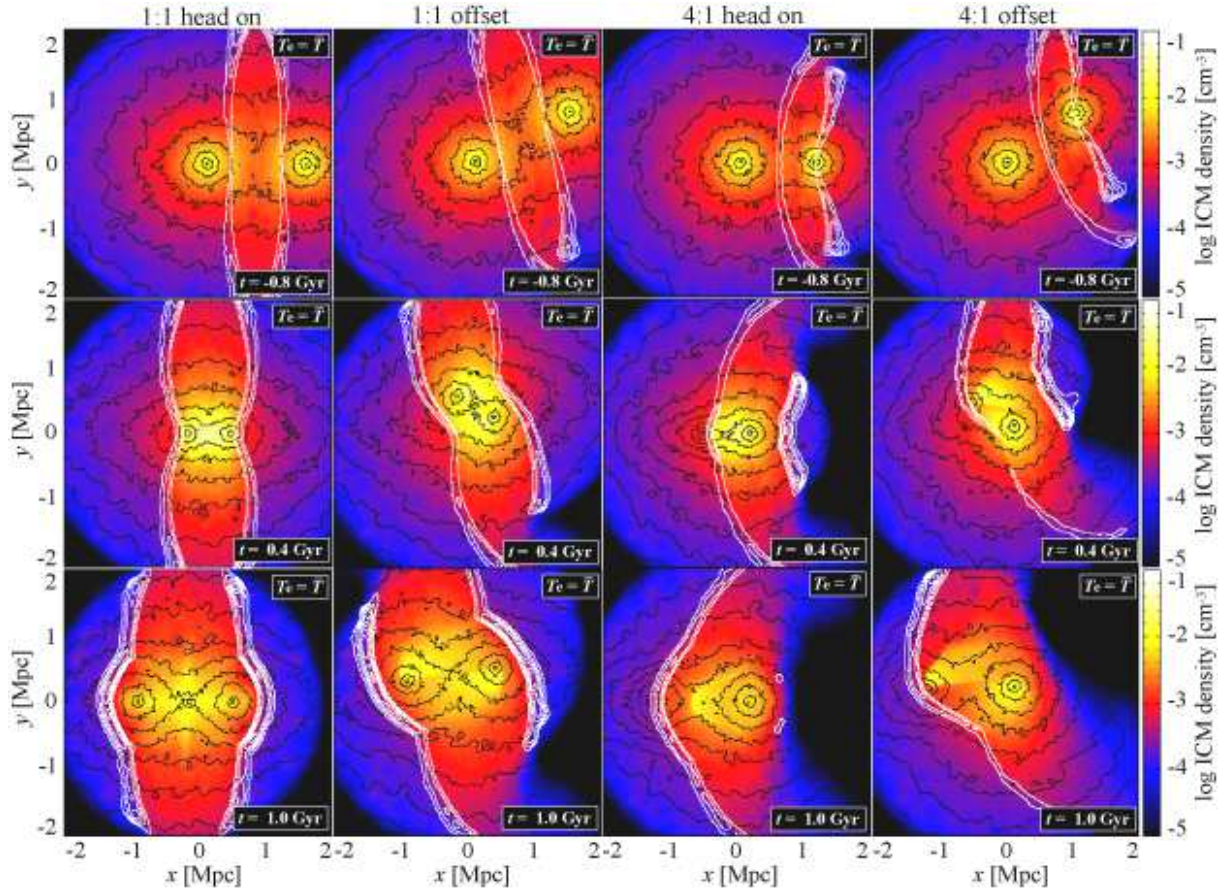


Fig. 2. Density maps of ICM on a collision plane of the two galaxy clusters are shown for 1:1 head on, 1:1 offset, 4:1 head on, and 4:1 offset (from the left to the right) at a time of $t = -0.8$ Gyr, 0.4 Gyr, and 1.0 Gyr (from the top to the bottom), respectively, where $t = 0$ Gyr corresponds to the time of the closest approach of the centers of the dark matter halos. White contours indicate the Mach number distribution of ICM for a Mach number of 1.5 and above, and are separated by a difference of 0.5. The distributions of dark matter are also overlaid with black contours.

the ionization fraction of Fe XXV is the largest among all the ionization states of iron, if ICM is in the ionization equilibrium (see figure 4). Therefore, in the rest of this work, we mainly focus on the ionization fraction of Fe XXV to address the degree of the deviation from the ionization equilibrium in ICM. The middle and bottom panels of figure 3 show the maps of the ionization fraction of Fe XXV, $f(\text{Fe XXV})$, at the late stage obtained in our simulations by integrating equation (8), and the ratio of the fraction of Fe XXV relative to that in the ionization equilibrium state, $f(\text{Fe XXV})/f_{\text{eq}}(\text{Fe XXV})$, respectively. Note that the fraction in the ionization equilibrium, $f_{\text{eq}}(\text{Fe XXV})$, is calculated using the mean temperature of electrons and ions, \bar{T} . It is clearly seen that we have a significant deviation from the ionization equilibrium state around the shock layers depicted in figure 2. The ratio of the ionization fractions, $f(\text{Fe XXV})/f_{\text{eq}}(\text{Fe XXV})$, is below unity and $\sim 0.6 - 0.8$ at the shock layers in the outskirts of galaxy clusters. On the other hand, it is greater than unity at the shocks in the central regions, and is $\sim 1.5 - 2.5$ and ~ 1.5 in the runs with 1:1 and 4:1 mass ratios, respectively.

The lack of the Fe XXV fraction at the shocks in the outskirts can be understood as follows. In these regions, the

shock heating increases the ICM temperature to ~ 3 keV from the lower temperature, so that the Fe XXV fraction in the post-shock regions increases with time toward the equilibrium fraction, because the Fe XXV fraction is maximum at ~ 3 keV in the ionization equilibrium state (see figure 4). However, the ionization to Fe XXV from lower-ionized states is not quick enough to catch up with the ionization equilibrium state. Therefore, the fraction of Fe XXV is lower than that in the ionization equilibrium state. On the other hand, at the shocks in the central regions, the ionization of Fe XXV to the higher ionization levels is not quick enough as well, leaving the Fe XXV fraction higher than that in the ionization equilibrium state. Actually, the fraction of Fe XXVI at the shocks in the central regions is lower than that in the ionization equilibrium state, and $f(\text{Fe XXVI})/f_{\text{eq}}(\text{Fe XXVI})$ is ~ 0.7 irrespective of the mass ratios.

3.2. Two-Temperature Runs

In this subsection, we show the results for the two-temperature runs, in which the assumption that electrons and ions share a single temperature is relaxed, in order to examine the effect of the two-temperature structure on

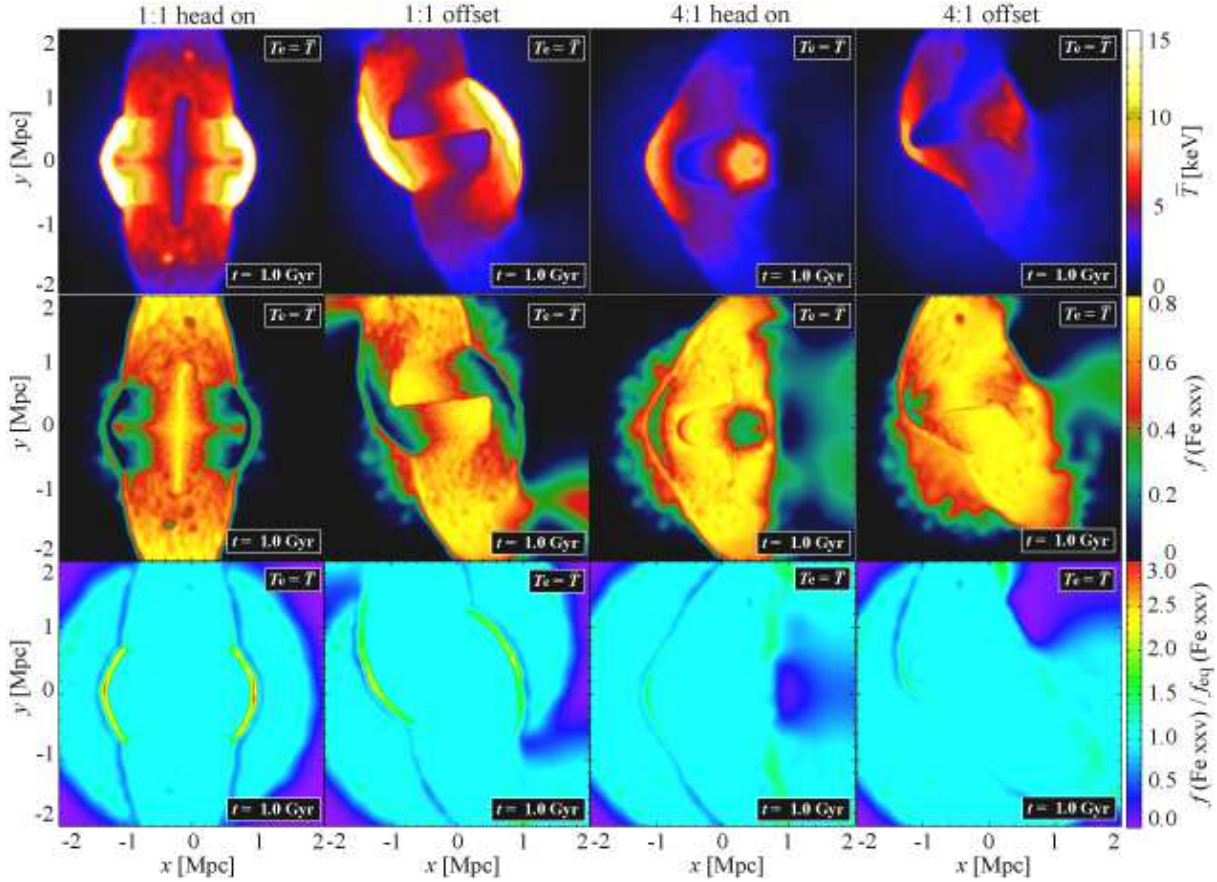


Fig. 3. The gas mean temperature, \bar{T} , the ionization fractions of FeXXV, and the ratio of the ionization fraction of FeXXV relative to that in the ionization equilibrium state (from the top to the bottom) on a collision plane of the two merging galaxy clusters in the runs, 1:1 head on, 1:1 offset, 4:1 head on, and 4:1 offset (from the left to the right), at a time of $t = 1.0$ Gyr.

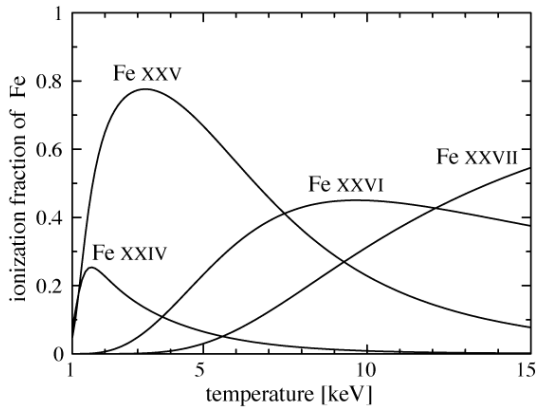


Fig. 4. Ionization fractions of Fe in the ionization equilibrium state as a function of temperature.

the ionization state of ICM. The thermal relaxation between electrons and ions is solved using equation (7). The simulations are performed for the same set of the initial conditions as the single-temperature runs.

The upper panels of figure 5 depict the maps of the ratio of the electron temperature relative to the mean temperature of ICM, T_e/\bar{T} , on the collision plane at a time of

$t = 1.0$ Gyr. It can be seen that the electron temperature is typically ~ 10 – 20 % lower than the mean temperature at the shocks in the outskirts, and ~ 50 % and ~ 25 % lower at the shocks in the central regions in the runs with a mass ratio of 1:1 and 4:1, respectively. In the runs with 1:1 mass ratio, we have a higher Mach number and a larger jump of the ion temperature at the shock layers than the runs with 4:1 mass ratio, and accordingly the larger temperature difference between electrons and ions.

Since the ionization and recombination rates in equation (8) depend on the electron temperature, the ionization states at the shocks in the two-temperature runs are altered from the results in the single-temperature runs in which the ionization and recombination rates are computed using the mean temperature, \bar{T} . The lower panels of figure 5 show the ratio of FeXXV fractions $f^{2T}(\text{FeXXV})$ in the two-temperature runs relative to $f_{\text{eq}}(\text{FeXXV})$, which is computed using the mean temperature, \bar{T} . Comparing the bottom panels of figure 3 and 5, we can see that the fraction of FeXXV is larger than that in the single-temperature runs at the shocks in the central regions. This is because a delay of the heating of electrons at the shocks leaves FeXXV fraction higher than that in the single-temperature runs. In other words, the electron temperature in the two-temperature runs (6–7 keV) is lower than that in the

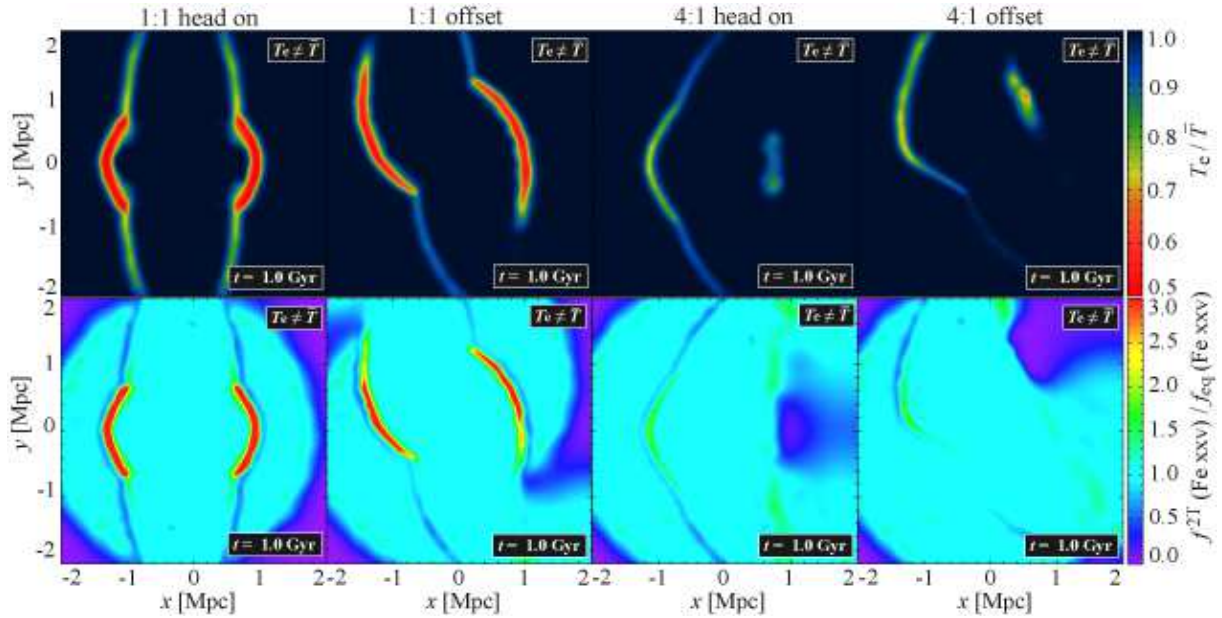


Fig. 5. The ratio of the electron temperature relative to the gas mean temperature, T_e/\bar{T} , (upper) and the ratio of the ionization fractions of FeXXV relative to that in the ionization equilibrium state (lower) on a collision plane of the two merging galaxy clusters in the runs 1:1 head on, 1:1 offset, 4:1 head on, and 4:1 offset (from the left to the right), at the late stage of the mergers ($t = 1.0$ Gyr) in the two-temperature runs.

single-temperature runs (9 – 14 keV), and thus the ionization rate of FeXXV to the higher ionization levels is significantly smaller.

3.3. Line Intensity Ratio

Here, let us consider observational imprints of the deviation from the ionization equilibrium and the difference in the temperature between electrons and ions in the X-ray spectroscopic observations. X-ray spectra of the simulated galaxy clusters are computed with the simulated ionization state and the hydrodynamical properties of ICM by utilizing the SPEX ver 1.10 software. In order to characterize the signatures of the non-equilibrium ionization state, we focus on the intensity of Fe K α line emissions which is usually adopted as a diagnostic feature of the ICM metallicity in X-ray observations, and introduce a ratio of the X-ray intensity between the two energy bands defined as

$$R = \frac{I(6.6 - 6.7 \text{ keV})}{I(6.9 - 7.0 \text{ keV})}, \quad (11)$$

where $I(6.6 - 6.7 \text{ keV})$ and $I(6.9 - 7.0 \text{ keV})$ are mainly contributed by the intensities of K α emissions from FeXXIV-XXV and FeXXVI, respectively. Since the contribution of FeXXIV K α emission to $I(6.6 - 6.7 \text{ keV})$ is minor for $f(\text{FeXXIV}) \lesssim 0.2$, the ratio R roughly reflects the ratio of K α line emission intensity between FeXXV and FeXXVI. Then, we introduce a ratio, R/R_{eq} , as a plausible tracer of the deviation from the ionization equilibrium, where R_{eq} is the intensity ratio under the assumption of the ionization equilibrium and thermal equipartition between electrons and ions. Note that R/R_{eq} is independent of the local ICM metallicity.

Figure 6 shows the map of R/R_{eq} of the simulated clusters at a time of $t = 1.0$ Gyr in the single- and two-temperature runs viewed along the line of sight perpendicular to the collision plane. It is clearly seen that R/R_{eq} significantly exceeds unity at the shocks in the central regions, and is slightly below unity at the shocks in the outskirts. These results are consistent with the fact that FeXXV is over- and underpopulated compared with the ionization equilibrium state at the shocks in the central regions and in the outskirts, respectively. The deviation of R/R_{eq} from unity in the two-temperature runs is larger than that in the single-temperature runs in accordance with the fact that the departure from the ionization equilibrium state in the two-temperature runs is larger than that in the single-temperature runs. Furthermore, since the difference in temperature between electrons and ions is larger at the shocks in the central regions than at the shocks in the outskirts, we have significant difference in R/R_{eq} between the single- and two-temperature runs primarily at the shocks in the central regions.

Maps of R/R_{eq} in the two-temperature runs viewed from different viewing angles (30 and 60 degrees) are shown in figure 7. Compared with the maps of R/R_{eq} for a viewing angle of 0 degree in figure 6, the deviation of R/R_{eq} from unity is significantly smaller for a viewing angle of 30 degrees, and almost negligible for a viewing angle of 60 degrees. This is because the shock layers where the ionization state deviates from the equilibrium state have geometrically thin structure and are almost perpendicular to the collision plane. Therefore, when viewed from a finite viewing angles, the signatures of the deviation from the ionization equilibrium are diluted by the surrounding

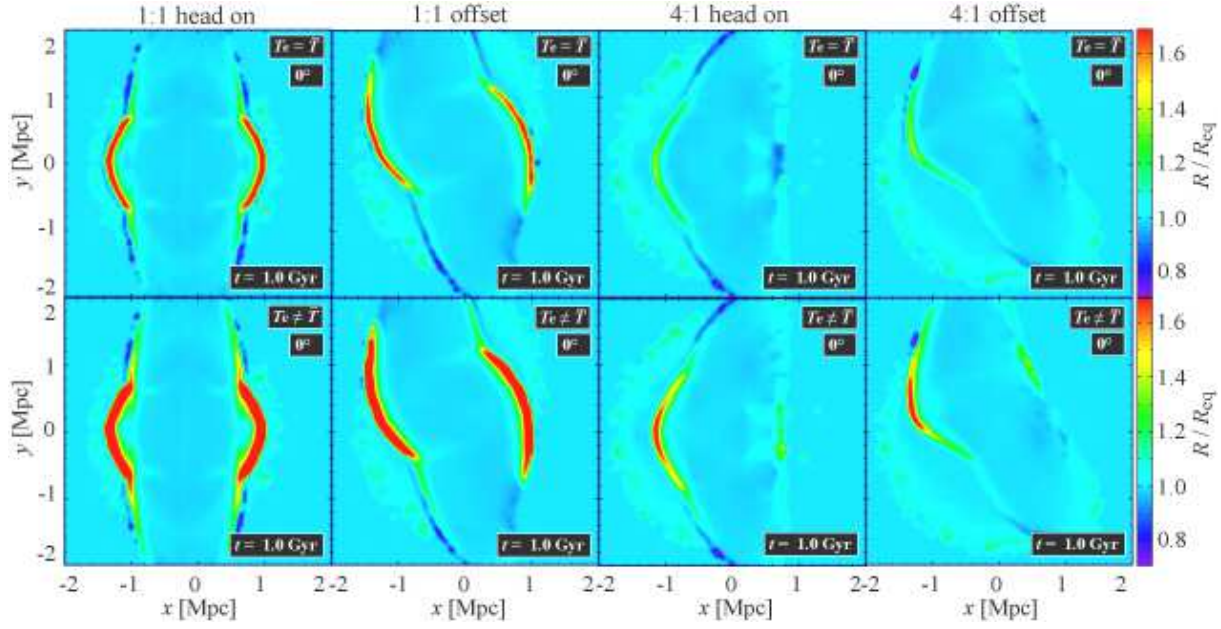


Fig. 6. The ratio, R/R_{eq} for the runs 1:1 head on, 1:1 offset, 4:1 head on, and 4:1 offset (from the left to the right), at $t = 1.0$ Gyr in the single- (upper) and two-temperature (lower) runs.

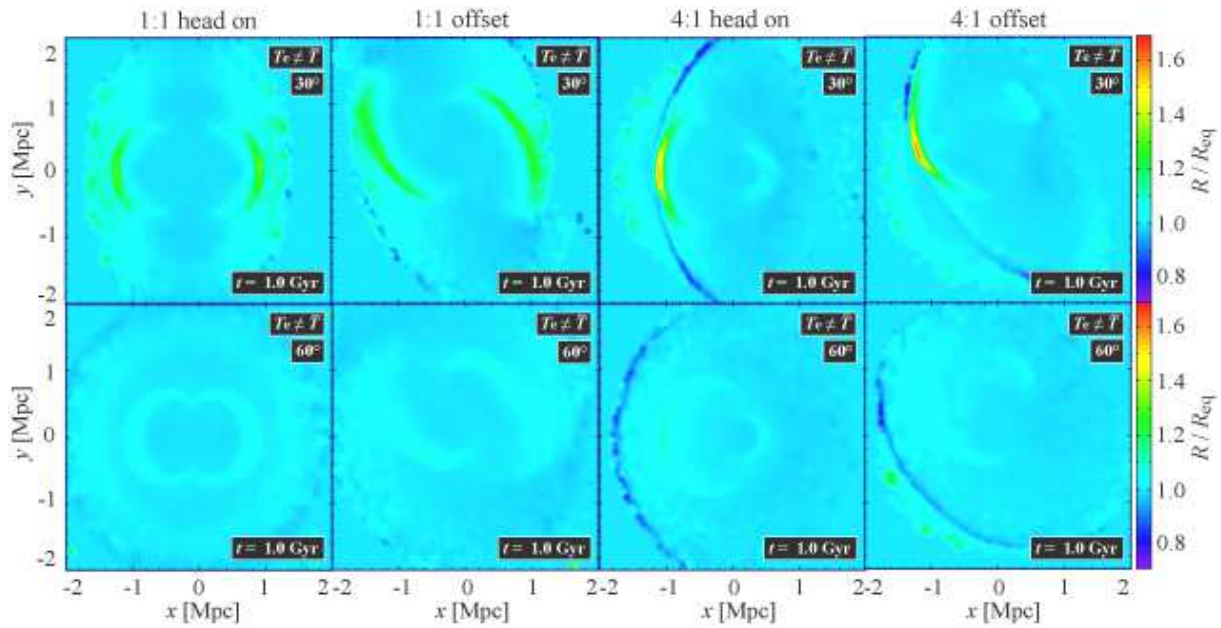


Fig. 7. Same as figure 6 but with viewing angles of 30 degrees (upper) and 60 degrees (lower) in the two-temperature runs.

ICM which is almost in the ionization equilibrium state.

3.4. Projected Temperature and X-ray Surface Brightness

Finally, let us consider the projected temperature and the X-ray surface brightness in the merging galaxy clusters. Observed temperature of ICM estimated by the X-ray spectrum fitting is generally different from its physical temperature due to the projection effect along the line of sight and the characteristic response of X-ray detectors. Here, we adopt the spectroscopic-like temperature (Mazzotta et al. 2004) as an estimate of the observed projected temperature of ICM.

Figure 8 shows the maps of the spectroscopic-like temperature and the X-ray surface brightness viewed from different viewing angles at a time of $t = 1.0$ Gyr. For a viewing angle of 0 degree, jumps of the spectroscopic-like temperature across the shocks are $\sim 4 - 7$ keV in the central regions and ~ 2 keV in the outskirts. When viewed from a viewing angle of 30 or 60 degrees, the jumps of the brightness and the projected temperature across the shock fronts are blurred, because the shock fronts are not aligned with the line of sight. Therefore, the Mach number estimated with the jumps of the observed temperature could be biased. Actually, the apparent jumps of the spectroscopic-like temperature in the case of 1:1 head on runs viewed with a viewing angle of 30 and 60 degrees are $\simeq 3$ keV and $\simeq 1$ keV, respectively, rather than the actual jumps of the electron temperature across the shock fronts $\simeq 5$ keV. The Mach numbers inferred from these apparent jumps of the projected temperature are 2.0 and 1.3, respectively, while the actual Mach number is ~ 4 .

4. Summary and Discussion

We carry out N-body + SPH simulations of merging galaxy clusters with various set of initial conditions by relaxing the assumptions of both the ionization equilibrium and thermal equilibration between electrons and ions in order to investigate the ionization state of ICM in the merging galaxy clusters in detail. As for the thermal equipartition between electrons and ions, we perform the single- and two-temperature runs to bracket the plausible theoretical uncertainties regarding the thermal relaxation processes between electrons and ions.

In our simulations, we find that the shocks induced by the merging events can be classified into two types regardless of the initial conditions. The first ones are formed at the early stage of the merging processes in the outskirts of the clusters where the sound velocity is roughly equal to or lower than the initial relative velocity of the merging galaxy clusters, and the second ones are formed in front of the dense cores of ICM in the late stage. Since the cores of ICM is accelerated by the gravitational potential of collisionless dark matter, the Mach number of the shocks in the central regions is higher than that in the outskirts.

It is shown that the ionization state of iron around these shocks deviates from the ionization equilibrium state. More specifically, the fraction of Fe XXV, the most pop-

ulated ionization state of iron in typical galaxy clusters, exceeds its ionization fraction in the ionization equilibrium at the shock layers in the central regions, while the fraction at the shock layers in the outskirts is lower than the equilibrium value. Both of these phenomena can be understood by the facts that the ionization processes at the shock layers are not quick enough to achieve the ionization equilibrium instantaneously and that the ionization state there differs from the equilibrium state for a while after experiencing the shock heating. Furthermore, in the two-temperature runs, the electron temperature at the shock layers are remarkably lower than the mean ICM temperature, and thus the deviation from the ionization equilibrium state is more significant than that in the single-temperature runs, because the ionization processes at the shock layers are retarded due to the lower temperature of electrons.

From the observational point of view, the deviation from the ionization equilibrium can be identified by the difference between intensity ratios of Fe K α line emissions and that inferred from the ICM temperature estimated by the X-ray continuum spectra. We find that the ratio, R/R_{eq} , can be a good tracer of such a deviation from the ionization equilibrium. We also find that the appearance of such observational imprints of the non-equilibrium ionization state is very sensitive to the viewing angle of the merging galaxy clusters to the observers. R/R_{eq} is the largest if the merging galaxy clusters are observed along the line of sight perpendicular to the collision plane of the two clusters, because the shock layers are geometrically thin and are parallel to the line of sight. On the other hand, the significance of such imprints is weaker in the case of a viewing angle of 30 degrees, and almost negligible in the case of 60 degrees. It is found that jumps of the spectroscopic-like temperature across the shock front also depend on the viewing angle, and that it is underestimated in the case of finite viewing angles, suggesting that the Mach numbers estimated from the jumps of the observed temperature could be also underestimated.

While we concentrate only on the ionization state of Fe so far, detections of the deviation from the ionization equilibrium of other heavy elements could provide independent information on the physical properties of the shock waves. Among heavy elements other than Fe, Si is the most interesting from the observational point of view because the emission lines of Si XIII-XIV at a photon energy of $\simeq 2$ keV are relatively prominent. Actually, at the shocks in the outskirts the ionization fraction of Si XIV is 1.5 – 2.0 and 1.5 – 3.0 times larger than that in the ionization equilibrium state in the single- and two-temperature runs, respectively. Since the ionization fraction of Si XIV in the ionization equilibrium is maximum at a temperature of $\simeq 10^7$ K, and almost fully ionized at higher temperature, the observational signatures of the deviation from the ionization equilibrium could be seen in the outskirts rather than in the central regions.

With the current X-ray observational facilities, the separate detection of emission lines of Fe XXV and Fe XXVI, or the measurement of the ratio R/R_{eq} is still difficult

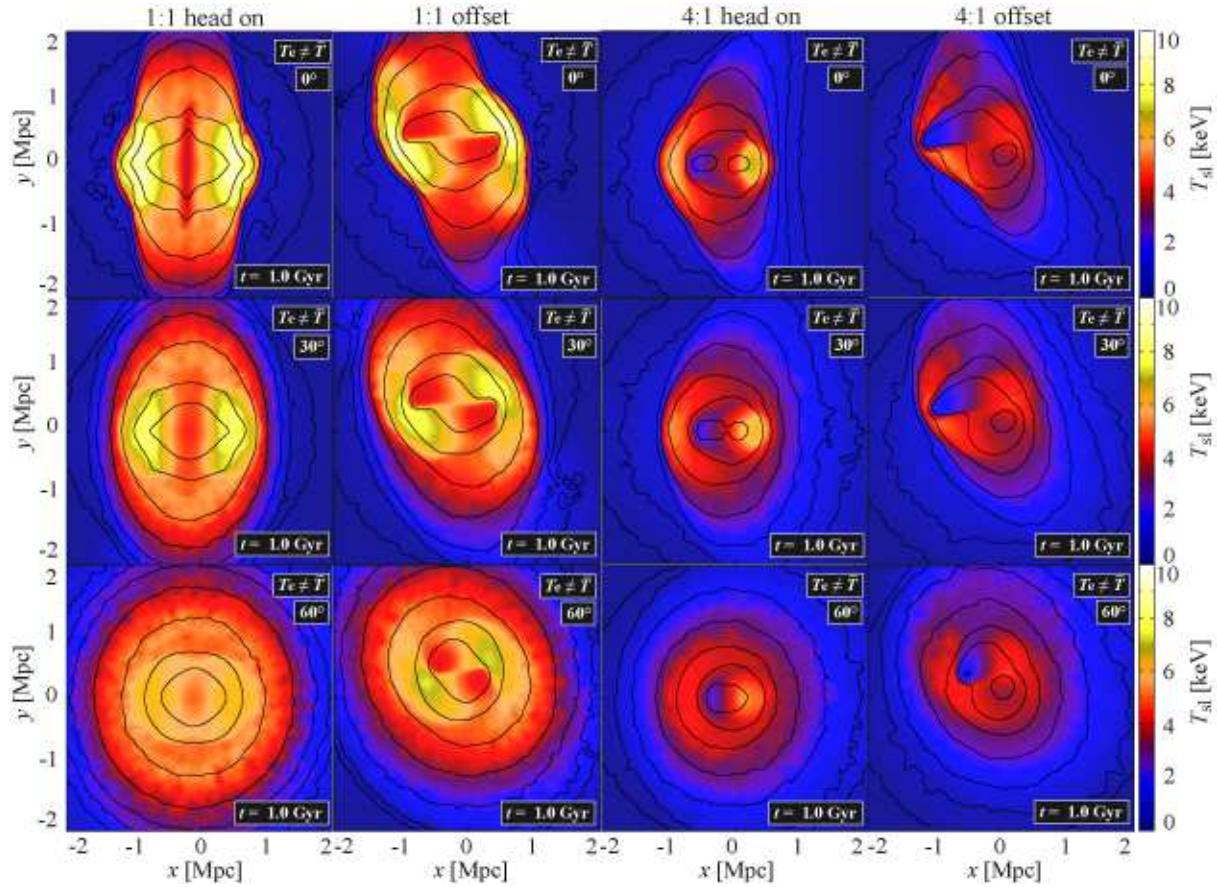


Fig. 8. The spectroscopic-like temperature map viewed with a viewing angle of 0, 30, and 60 degrees (from the top to the bottom), respectively, for the runs 1:1 head on, 1:1 offset, 4:1 head on, and 4:1 offset (from the left to the right), at $t = 1.0$ Gyr in the two-temperature runs. Black contours show the X-ray surface brightness.

because of a lack of the spectroscopic resolution of the CCDs. Therefore, spectroscopic analyses to estimate the metallicity of ICM with the assumption that ICM is in the ionization equilibrium state can lead to a biased result. A good spectroscopic resolution is also crucial to estimate the temperatures of electrons and ions separately, because the ion temperature is only estimated from the detailed line profiles of emission lines, while the electron temperature can be relatively easily estimated from the X-ray continuum spectra. Thus, the precision spectroscopy in X-ray observations is of crucial importance in studying the non-equilibrium ionization state and the two-temperature structure of ICM, and can be achieved by X-ray calorimeters on board future satellites such as Astro-H and International X-ray Observatory.

This work is supported in part by Grant-in-Aid for Specially Promoted Research (16002003) from MEXT of Japan, Grant-in-Aid for Scientific Research (S) (20224002), for Scientific Research (A) (20340041), for Young Scientists (Start-up) (19840008) and for Challenging Exploratory Research (21654026) from JSPS. Numerical simulations for the present work have been carried out under the “Interdisciplinary Computational Science Program” in Center for Computational Sciences,

University of Tsukuba. TA is supported in part by Korea Science and Engineering Foundation (R01-2007-000-20196-0).

References

- Akahori, T., & Masai, K. 2005, PASJ, 57, 419
- Akahori, T., & Masai, K. 2006, PASJ, 58, 521
- Akahori, T., & Yoshikawa, K. 2008, PASJ, 60, L19 (AY08)
- Balsara, D. S. 1995, J. Comput. Phys., 121, 357
- Cavaliere, A., & Fusco-Femiano, R. 1976, A&A, 49, 137
- Cen, R., & Fang, T. 2006, ApJ, 650, 573
- Fox, D. C., & Loeb, A. 1997, ApJ, 491, 459
- Fujita, Y., Tawa, N., Hayashida, K., Takizawa, M., Matsumoto, H., Okabe, N., & Reiprich, T. H. 2008, PASJ, 60, S343
- Ghavamian, P., Laming, J. M., & Rakowski, C. E. 2007, ApJL, 654, L69
- Masai, K. 1984, Ap&SS, 98, 367
- Mazzotta, P., Rasia, E., Moscardini, L., & Tormen, G. 2004, MNRAS, 354, 10
- Monaghan, J. J., & Gingold, R. A. 1983, J. Comput. Phys., 52, 374
- Navarro, F. J., Frenk, C. S., & White, S. D. M. 1997, ApJ, 490, 493
- Pfrommer, C., Springel, V., Enßlin, T. A., & Jubelgas, M.

- 2006, MNRAS, 367, 113
- Ricker, P. M., & Sarazin, C. 2001, ApJ, 561, 621
- Ritchie, B. W., & Thomas, P. A. 2002, MNRAS, 329, 675
- Roettiger, K., Loken, C., & Burns, J. 1997, ApJS, 109, 307
- Rudd, D. H., & Nagai, D. 2009, ApJL, 701, L16
- Ryu, D., Kang, H., Hallman, E., & Jones, T. W. 2003, ApJ, 593, 599
- Sarazin, C. 2002, Merging Processes in Clusters of Galaxies, ed. Feretti, L., Gioia, I. M., & Giovannini, G. (Dordrecht: Kluwer Academic Publishers), Astrophysics and Space Science Library, 272, 1
- Spitzer, L. Jr. 1962, Physics of Fully Ionized Gases (New York: Wiley)
- Springel, V., & Hernquist, L. 2002, MNRAS, 333, 649
- Takizawa, M. 1999, ApJ, 520, 514
- Takizawa, M. 2000, ApJ, 532, 183
- Takizawa, M. 2005, ApJ, 629, 791
- Takizawa, M. 2006, PASJ, 58, 925
- Vikhlinin, A., Markevitch, M., Murray, S. S., Jones, C., Forman, W., & Van Speybroeck, L. 2005, ApJ, 628, 655
- Yoshida, N., Furlanetto, S. R., & Hernquist, L. 2005, ApJ, 618, L91
- Yoshikawa, K., & Sasaki, S. 2006, PASJ, 58, 641